Transcriptome-wide mapping of small ribosomal subunits elucidates scanning mechanisms of translation initiation in the mammalian brain

Preeti M Kute[1,2,†], Francois P Pauzin[3,†], Kornel Labun[1,†], Clive R Bramham[3,4,*], Eivind Valen[1,2,5,*]

1. Computational Biology Unit, Department of Informatics, University of Bergen, Bergen, Norway
2. Michael Sars Centre, University of Bergen, Bergen, Norway
3. Department of Biomedicine, Jonas Lies vei 91, University of Bergen, Bergen, Norway
4. Mohn Research Center for the Brain, University of Bergen, Bergen, Norway
5. Department of Biosciences, University of Oslo, Oslo, Norway

† shared first authors

* corresponding authors: clive.bramham@uib.no, eivind.valen@ibv.uio.no

Abstract

Protein synthesis in neurons is highly compartmentalised and regulated, with key roles for translation initiation and elongation factors. The most widely used transcriptome-wide method for measuring translation, ribosome profiling, characterises the elongation phase of translation but does not provide insight into the initiation phase with scanning of the small ribosomal subunit (SSU). Here, we adapted and optimised ribosome complex profiling (RCP-seq) for brain tissue, that captures SSUs and allows analysis of translation initiation dynamics in the adult murine dentate gyrus (DG) region of the hippocampus. We show an accumulation of SSUs upstream of the start codon specifically enriched on synaptically localised RNAs and extensive translation of 5' upstream open reading frames (uORFs), suggesting regulation both during scanning and transition to the elongation phase. We further demonstrate that neuron-specific transcripts are more expressed, scanned, and translated than glia-specific transcripts. Of the neuronal mRNAs, monosome-preferring mRNAs exhibited reduced scanning and elongation relative to polysome-preferring transcripts implying reduced recruitment of ribosomes. In sum, RCP-seq

elucidates translation initiation dynamics in the mammalian brain and uncovers cell-type- and transcript-specific regulation.

Keywords: small ribosomal subunit, ribosome complex profiling, translation initiation, elongation, dentate gyrus.

Introduction

Eukaryotic translation can be divided into four distinct stages: initiation, elongation, termination, and ribosome recycling. However, knowledge of translation dynamics across these stages is limited due to the lack of methods with nucleotide resolution in live systems (Hinnebusch 2014; Sokabe and Fraser 2019; Merrick and Pavitt 2018; Larsson, Tian, and Sonenberg 2013). Translation initiation, a rate-limiting process in protein synthesis, can be further divided into recruitment, scanning, and start codon recognition, each stage of which can be subject to regulation. During recruitment, the assembly of the preinitiation complex (PIC) containing the small ribosomal subunit (SSU/40S) with methionyl-initiator tRNA, and subsequent recruitment to the mRNA 5' cap, is regulated by eukaryotic initiation factors (eIFs) (Hinnebusch 2014). Following recruitment, the PIC scans the 5' leader for a start codon, after which the large ribosomal subunit (LSU/60S) joins the SSU to form an elongation-competent ribosome (80S).

Translation in neurons is highly compartmentalised and regulated due to their complex polar structure and function. A prominent example is the local translation in the synaptic compartment remote from the cell body, important for synapse development, maintenance, and plasticity (Holt, Martin, and Schuman 2019; Bramham and Wells 2007; Sun and Schuman 2023). Both translation initiation and elongation in the nervous system are modulated by changes in translation factor activity in response to changes in neural activity and neurotransmitter receptor activation. Converging evidence highlights the role of translation initiation factors (eIF2α, eIF4E) as regulators of protein synthesis in synaptic plasticity and diverse functions such as circadian rhythms, social behaviour, memory, and cognitive flexibility

(Patil et al. 2023; Amorim et al. 2018; Cao et al. 2015; Sharma et al. 2020; Moon, Sonenberg, and Parker 2018; Oliveira and Klann 2022). While these studies demonstrate the role of initiation factors in PIC recruitment and 5' leader scanning, they do not provide insights into the later phases, the 5' leader scanning and start codon recognition.

Analysing 80S ribosome-bound mRNAs through ribosome profiling and related techniques such as TRAP-seq has provided insight into many questions related to translation control in the mammalian brain (Thomson et al. 2017; Hien et al. 2020; Amorim et al. 2018). However, ribosome profiling characterises only the elongation step of translation such that the dynamics and regulation of translation initiation in the mammalian nervous system have remained elusive. Translation complex profiling (TCP-seq) was the first method to characterise the occupancy of SSUs across the transcriptome (Archer et al. 2016). This was used to explore translation initiation in yeast and was later followed by a modified technique, ribosome complex profiling (RCP-seq), to explore initiation in the early development of zebrafish (Giess et al. 2020). In the mammalian brain, however, transcriptome-wide characterization of translation initiation has not been attempted.

Here we developed a UV light crosslinking method capable of producing sufficient input material for RCP-seq for the mice brain tissues. This approach generated libraries of similar quality to previous studies (Archer et al. 2016; Giess et al. 2020) and allowed a detailed characterization of translation initiation and elongation in the nervous system for the first time. Using the DG region of the hippocampus from mice forebrain, we show regulation of translation at all stages of initiation. First, SSUs accumulate upstream of the start codon in a poised state on synaptically-localised mRNAs, indicating a novel regulatory step during the transition to the elongation step. Second, our data reveals regulation during scanning with a role for uORF-mediated translational repression of the downstream CDS. Third, we show that neuron-enriched transcripts are relatively more expressed, scanned, and translated relative to glia-enriched transcripts. Finally, RCP-seq uncovers that neuronal transcripts preferring monosomal translation have reduced recruitment of ribosomes leading to lower translation efficiencies.

Results

Mapping the SSU and 80S ribosomal complexes in the dentate gyrus of the adult mouse brain

Previous methods for capturing scanning SSUs have used formaldehyde and chemical crosslinking for the SSU fixation to obtain footprints on the mRNAs (Archer et al. 2016; Bohlen et al. 2020; Giess et al. 2020; Wagner et al. 2020). In mouse brain tissue, the use of 0.1% or 0.05% formaldehyde resulted in less crosslinking for polysomes as compared to UV-crosslinked lysates (**Supplementary figure 1a**). Thus, we opted for UV-crosslinking, which has been previously used for studying RNA binding protein (RBP) interactions with mRNAs (Hafner et al. 2021) and for polysome profiling in the brain tissue (Darnell et al. 2011) (**Supplementary figure 1a**). The steps to efficiently crosslink the SSU and the 80S on RNAs from the mouse brain tissue are outlined in **Figure 1a** and detailed in the methods section. Briefly, the pre-cleared lysate was exposed to UV irradiation and digested with RNase I to obtain footprints (**Supplementary figure 1b**). The fractions corresponding to the SSU and 80S were collected post-digestion and libraries were prepared and sequenced to 20-130 million reads per library (**Supplementary table 1**). Total RNA libraries were prepared from matched undigested samples to estimate RNA abundance.

The library quality was comparable to previous studies (Archer et al. 2016; Giess et al. 2020) where contaminants were largely from rRNAs and ncRNAs (**Supplementary figures 1c**). Of the SSU reads mapped to mRNAs, 52% mapped to the 5' leader (**Figure 1b**) while 94% of the 80S reads mapped to the coding sequence (CDS) (**Figure 1b**). Accordingly, when normalised to the expected fraction of reads from a given region, estimated from the total mRNA library, the SSU libraries and 80S libraries were enriched in the 5' leader and CDS respectively. (**Figure 1c**). Footprint length distribution for the 80S libraries was within the expected range: 26-30 nt (Ingolia et al. 2009); Similarly, SSU footprints had a broader distribution with many longer fragments, 20-75 nt in these libraries (**Supplementary figure 1e**) as previously reported (Giess et al. 2020; Archer et al. 2016). Metagene heatmaps of SSU footprints over the translation initiation site (TIS) for the DG showed a range of fragment lengths (20-75 nt) forming a diagonal preceding the TIS (**Figure 1d**). This has been attributed to longer pre-initiation complex

conformations due to the presence of initiation factors (Bohlen et al. 2020; Archer et al. 2016). Some SSU footprints are also present internally in the CDS, potentially representing contamination from dissociated 80S ribosomes during sample preparation or instances of “leaky scanning” where the PIC scans through the start codon and into the CDS. For the 80S ribosomes **(Figures 1f and 1g)**, the footprints are enriched at the TIS and show the expected 3-nucleotide periodicity throughout the CDS. Replicates were highly correlated (**Supplementary figures 1f-1h**) and clustered separately as SSU, 80S, and RNA (**Supplementary figure 1i**) with PCA, demonstrating the robustness and reproducibility of the method. To check the transferability of the technique, we additionally applied RCP-seq to another brain tissue, the cerebral cortex. The results of this are discussed in the last section of results. Taken together, the UV-crosslinking method successfully captures the SSU and 80S ribosomal complexes transcriptome-wide in the adult mouse DG region of the hippocampus and in the cerebral cortex.

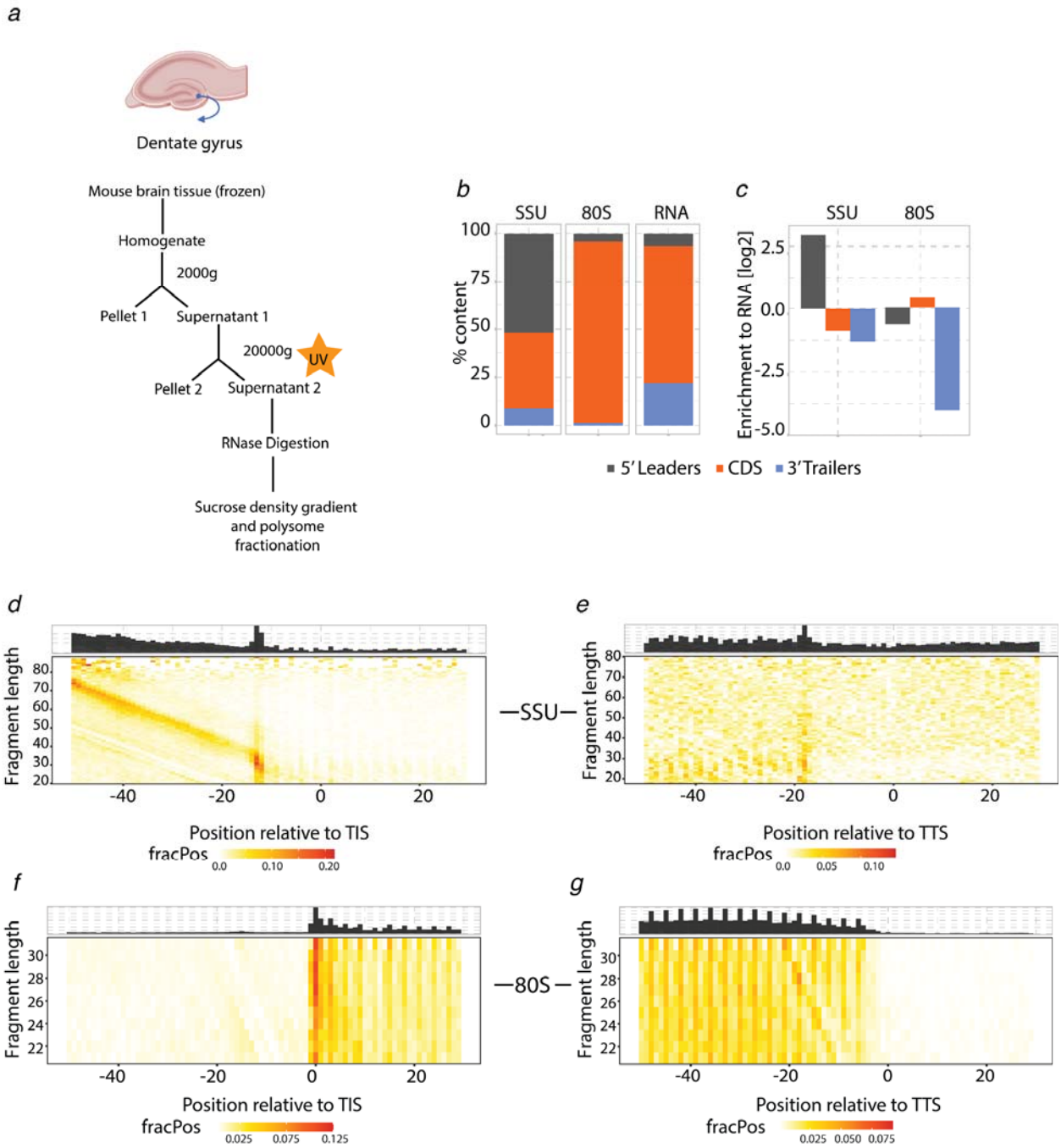

Figure 1: Ribosome complex profiling (RCP-seq) captures small ribosomal subunits (SSU) and elongating ribosomes (80S) from the mouse DG tissue.

a: Steps for ribosomal complex profiling using UV crosslinking for the fixation of the SSU and 80S in the DG.

b and **c**: Content plots displaying the mapping of SSU, 80S, and total mRNA counts to the 5' leaders, CDS, and 3' trailers of the transcripts. **b** shows the % count for each library and **c** displays the normalised counts to the total RNA.

d-e: Footprint length distribution for the 5' end of SSU fragments in the DG for **d)** translation initiation site (TIS) and **e)** translation termination site (TTS). FracPos indicates the fraction of counts per position per gene.

f-g: Footprint length distribution for the 5' end of 80S fragments in the DG for **f)** translation initiation site (TIS) and **g)** translation termination site (TTS). FracPos indicates the fraction of counts per position per gene.

Poised SSUs upstream of TIS in selected genes

The footprints upstream of the TIS revealed an accumulation of SSUs proximal to the start codon (**Figure 1d**). Increased resolution of this phenomenon showed that these SSU fragments are approximately 60 nt long and reside around 40 nt upstream of the TIS (**Figure 2a**). Longer fragments from SSU footprinting in yeast and zebrafish embryos have previously been explained as pre-initiation complexes associated with initiation factors that extend the protection on RNA (Archer et al. 2016; Giess et al. 2020). However, in mouse brain tissue we noted that the position (-40 nt) and length (60 nt) of the enriched transcripts also correspond exactly to two SSU units positioned back-to-back (**Figure 2b**). While sequencing data does not resolve the basis of longer SSU footprints, it demonstrates the accumulation of SSUs on 5' leaders at a specific position upstream of the TIS. We refer to this population of SSU complexes as "poised SSUs" due to them being poised to transition to the elongation state.

We next asked where and to what extent poising occurs in the transcriptome. As poised SSUs overlap the start codon, they cannot coexist on the same transcript with the short SSU conformations at -12 nt that initiate elongation. The transition between these two conformations could therefore indicate a regulatory step before or during start codon recognition concomitant with a change in ribosomal conformational state. We, therefore, defined an "SSU poised ratio" as the ratio between the two mutually exclusive configurations of poised SSUs and initiating SSUs (boundaries in **Figure 2a**) and calculated this metric for 2725 transcripts that had sufficient coverage of SSU reads, from the cortical and DG tissues. This revealed that most transcripts have more initiating SSUs than poised SSUs, but that a subset of transcripts have substantially higher poising (**Figure 2c,** below *vs*. above zero). We selected the strongest SSU-poised transcripts as those having a two-fold enrichment in poised *vs*. initiating SSUs (76 genes for DG and 198 for cortex) and the weakest as two-fold depletion (1536 genes for DG and 1041 for cortex). Further analysis revealed that poised genes generally have substantially more scanning activity with a higher occupancy of SSUs across the 5' leader, but a weaker presence of 80S ribosomes at the TIS

(**Figure 2d**). This could indicate increased recruitment of PIC to the RNA, potentially combined with either a slower joining of 60S or a faster translocation of 80S away from the TIS. We calculated the translation efficiency (TE, see methods) metric to assess the presence of 80S on these transcripts and observed higher translation efficiency for transcripts with high poising ratio as compared to those with low poising ratio (**Figure 2e**).

To probe the biological relevance of poised SSUs, we analysed the 42 genes poised in both DG (76 genes) and cortex (198 genes) tissues for overrepresented functional GO categories against a restrictive background of other genes with SSU poise ratio - 2725 genes (1917 DG, 1969 cortex) (**Supplementary table 2**). This revealed four enriched categories (**Figure 2f**) all belonging to the synaptic compartment of the neuron. A prominent gene is *Camk2α* (**Figures 2g and 2h**) where the SSU occupancy plot showed a strong enrichment of SSUs near and up to 60 nt upstream of TIS (**Figure 2h**). Other examples include *Clstn3*, *Pcbp2*, *Pacsin1*, *Rtn3*, *Prnp*, and *Prkcg* (**Supplementary figure 2a-2f**). Together this shows that poised SSUs are enriched in a subset of genes and that several of these are functionally related.

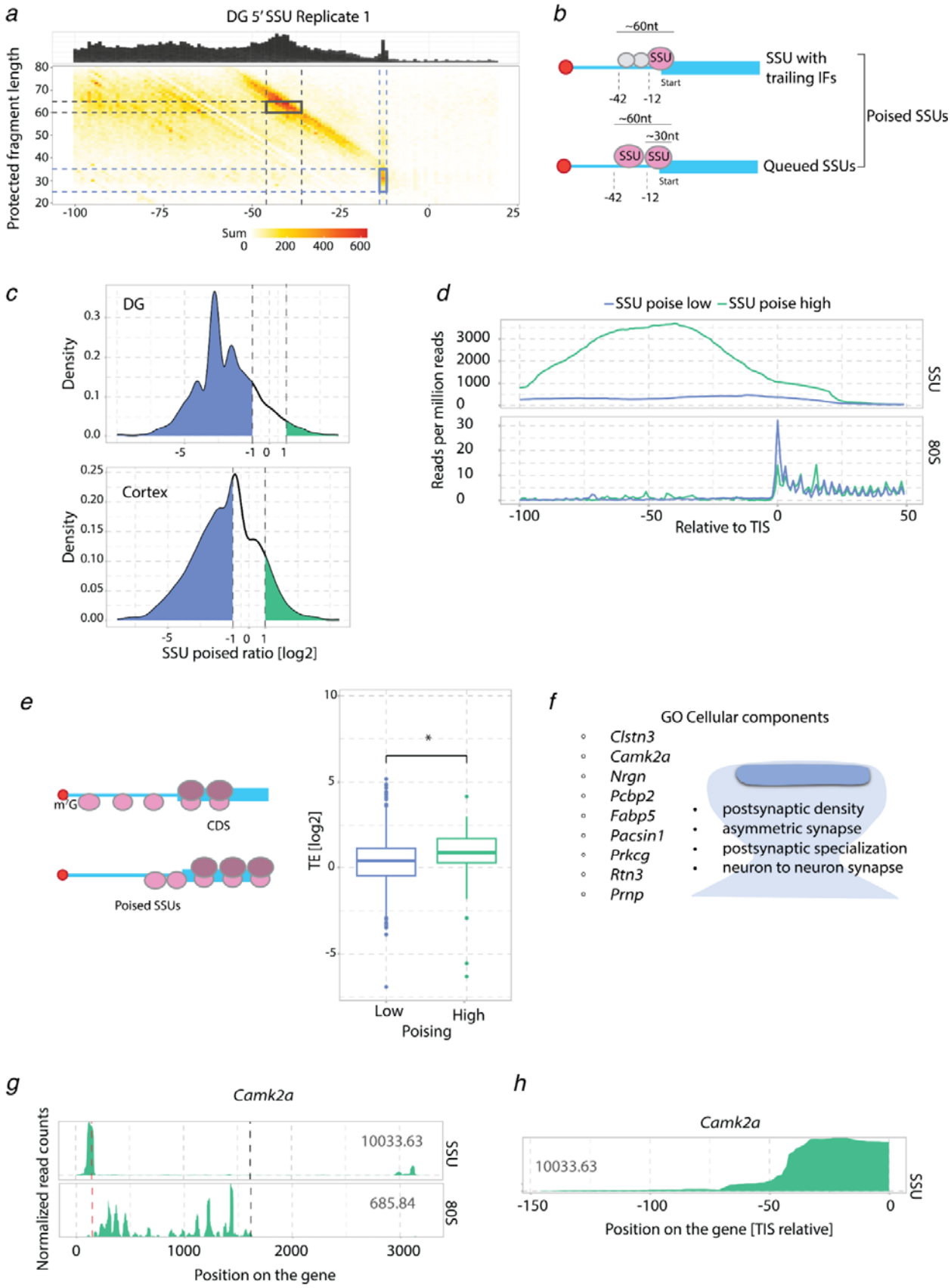
a
DG 5′ SSU Replicate 1
Protected fragment length
Sum
b
~60nt
SSU
Start
-42
-12
SSU with trailing IFs
~30nt
Queued SSUs
Poised SSUs
c
DG
Cortex
Density
SSU poised ratio [log2]
d
SSU poise low
SSU poise high
Reads per million reads
Relative to TIS
SSU
80S
e
m7G
CDS
Poised SSUs
TE [log2]
Low
High
Poising
f
GO Cellular components
Clstn3
Camk2a
Nrgn
Pcbp2
Fabp5
Pacsin1
Prkcg
Rtn3
Prnp
postsynaptic density
asymmetric synapse
postsynaptic specialization
neuron to neuron synapse
g
Camk2a
Normalized read counts
10033.63
685.84
Position on the gene
h
Camk2a
10033.63
Position on the gene [TIS relative]

Figure 2: SSU build-up observed in the leaders of transcripts in the DG.

a: Footprint length distribution for the 5' end of SSU fragments in the DG for the TIS, highlighting initiating SSUs (at -12nt) and poised SSUs (-46: -42nt).

b: Schematic of two conformations of poised SSUs near the TIS of transcripts with 60 nt length..

c: Distribution plot for SSU poised ratio (log2) for DG and cortical transcripts. Dotted lines indicate SSU poised ratio cut-off of -1 and +1. Coloured regions indicate transcripts with lower (blue) or higher (green) poised ratios from the cut-off lines.

d: Metagene coverage for transcripts with SSU poised ratio below (blue) or higher (green) than the cut-offs in the DG and cortex relative to the TIS.

e: Log2 of Translation Efficiency (TE) for genes with high or low poised ratios (FPKM based, t-test statistics) for DG and cortical transcripts.

f: GO enrichment categories for genes with SSU poising ratio more than 2 and the list of genes enriched in the categories in both DG and cortex.

g: Single gene profile for SSU and 80S, without intronic regions, and plotted for the longest isoform of *Camk2α*. Numbers indicate FPKM values. Dotted lines indicate TIS (red) and TTS (black).

h: Single gene profile for SSU within the 5' leader region of *Camk2α*. Numbers indicate FPKM values.

uORF-mediated regulation in the DG tissue

Upstream open reading frames (uORFs) are regions in the 5' leaders of mRNAs with a start codon and a downstream in-frame stop codon, potentially encoding a peptide. While many of these uORFs are translated, it is believed that most of these do not produce functional peptides but rather contribute to regulating translation of the downstream CDS (Dever, Ivanov, and Hinnebusch 2023; Kute et al. 2021). A key regulatory feature of uORFs is that some ribosomes detach after translating the uORF and therefore are unable to initiate at the TIS (**Figure 3a**), leading to translation downregulation of the CDS. To explore the role of uORFs in the translation regulation of downstream CDSs in the DG, we defined uORFs as ORFs with read coverage and having an ATG as the start codon. For those 5' leaders containing multiple eligible uORFs we selected the one with the highest read coverage (totaling 1062, see methods). These were termed as "active uORFs" (**Supplementary table 3**). To check the effect of the translation of uORFs on downstream CDS, we looked at the effect of the presence or absence of uORFs on the translation of the transcripts. This showed a modest but significant inhibitory effect of having actively translated uORFs (**Figure 3b**). To further explore the role of uORFs in regulation of CDS translation we calculated the scanning efficiency (SE) (**Figure 3c**) which quantifies the abundance of SSU occupancy in the leaders normalised to the RNA levels. SEs were comparable between transcripts

harbouring uORFs and those without, implying that uORFs do not globally have a significant effect on the overall occupancy of SSUs over the leaders (**Figure 3d**). On the other hand, uORFs can affect the SSU traversal over the 5' leaders either through slowing them by temporarily elongating a uORF or dissociating a proportion of them from the RNA after uORF translation. To check whether uORFs had any impact on the number of SSUs reaching the TIS, we looked at poised SSUs at the position -40 nt and length 60 nt for genes with and without uORFs. The poised SSUs reads were normalised to RNA to accommodate any differences at the RNA level. This analysis revealed that the poised SSUs in those genes containing an active uORF were significantly lower ($p<0.05$, unpaired t-test, **Figure 3e and 3f**) suggesting that uORFs may act to slow down or block SSUs on their way to the CDS.

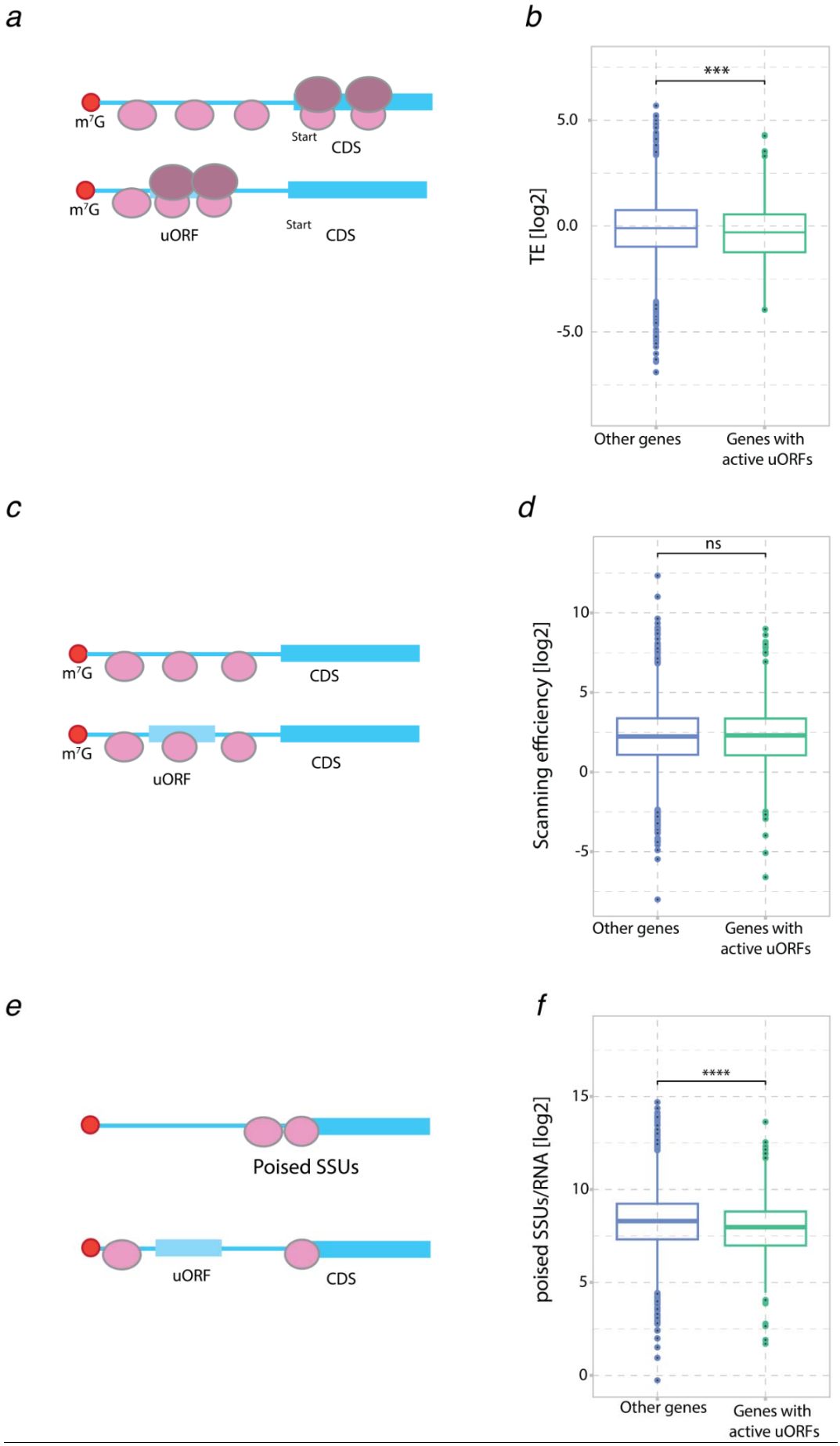
a
m7G
Start
CDS
m7G
uORF
Start
CDS
b
***
5.0
0.0
-5.0
TE [log2]
Other genes
Genes with active uORFs
c
m7G
CDS
m7G
uORF
CDS
d
ns
10
5
0
-5
Scanning efficiency [log2]
Other genes
Genes with active uORFs
e
Poised SSUs
uORF
CDS
f
****
15
10
5
0
poised SSUs/RNA [log2]
Other genes
Genes with active uORFs

Figure 3: uORF expression in the DG

a: Illustration explaining the role of uORFs on the translation of downstream CDS.

b: Comparison of CDS translation efficiency (TE) in relation to the presence or absence of active uORFs in DG (FPKM based, t-test statistics).

c: Illustration explaining the role of uORFs on the scanning efficiency (SE) of downstream CDS

d: Comparison of the SE in relation to the presence or absence of active uORFs in DG (FPKM based, t-test statistics).

e: Illustration explaining the role of uORFs on the SSU poising over 5' leaders

f: Comparison of the poised SSUs in relation to the presence or absence of active uORFs in DG (FPKM based, t-test statistics).

The translational landscape of neuronal and glial genes

The mammalian brain consists of both neuronal and non-neuronal cells such as astrocytes, oligodendrocytes, microglia, and blood vessel cells. To elucidate the translational landscape of cell-type specific transcripts, we filtered our dataset according to previously defined neuronal and glial-enriched transcripts (Glock et al. 2021). Interestingly, SSU and 80S footprints showed that neuronally-enriched transcripts are relatively more expressed, scanned and translated compared to glial-enriched transcripts (**Figure 4a**). Specifically, neuronal-enriched transcripts showed significantly higher TE and SE values as compared to glial-enriched transcripts (**Figures 4b and 4c**) indicating that protein synthesis is biased towards neuronal function. Examples of this can be seen when visualising the SSU and 80S occupancy profiles for two neuronal transcripts *C1ql2* and *Prox1* **(Figures 4d and 4e)**.

Taken together, the neuronal-enriched transcripts contain more SSU reads in their leaders, more 80S coverage in their CDS and are more abundant at the RNA level than glial-enriched transcripts. This suggests a major cell-type specific difference, with enhanced expression and translation of neuronal transcripts relative to glial transcripts in the DG.

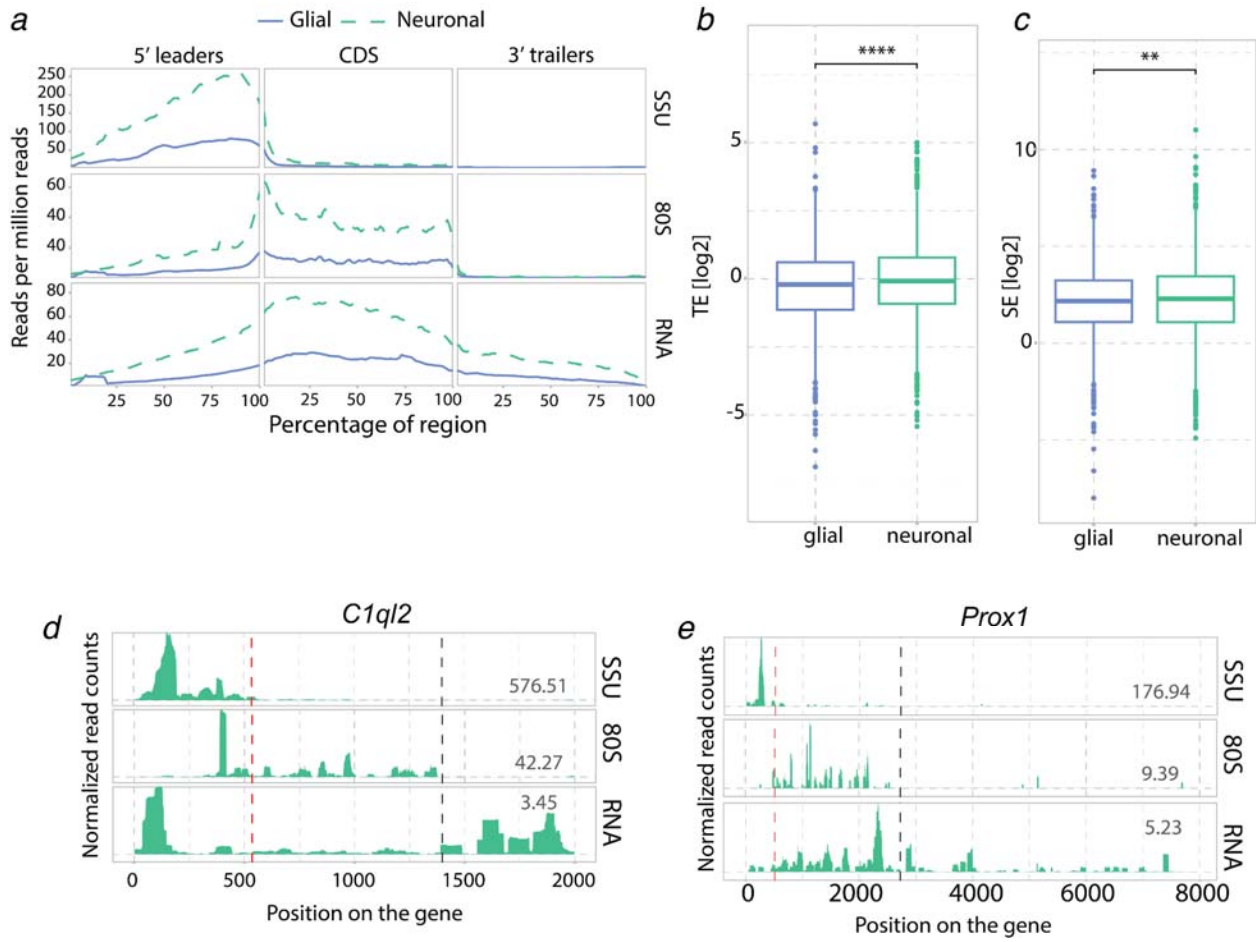

Figure 4: Transcriptional and translational profiles for neuronal and glial-specific genes in the DG of mouse hippocampus

a: Metagene coverage for the SSU, the 80S and total RNA between neuronal- and glial-enriched transcripts.

b and c: Translation efficiency and scanning efficiency for glial and neuronal-specific transcripts.

d-e: Single gene profiles for SSU, 80S and total RNA coverage, without intronic regions, and plotted for the longest isoform. **d**) *C1ql2* , **e**) *Prox1*. Numbers indicate FPKM values. Dotted lines indicate TIS (red) and TTS (black).

Scanning and elongation in neuropil-enriched monosome- *vs*. polysome-preferring transcripts

Since translation in neurons is compartmentalised, occurring even in distal dendrites, we next studied transcripts that are differentially localised and translated between the soma and the synaptic neuropil. In a previous study based on ribosome profiling, more than 800 transcripts were found to be predominantly translated in the neuropil (neuronal dendrites and axons) of microdissected rat hippocampal tissue slices (Glock et al. 2021). Surprisingly, a recent report based on polysomal profiling of microdissected hippocampal CA1 tissue showed that most of the neuropil translation is mediated by monosomes, with only one actively translating ribosome per transcript (Biever et al. 2020) (**Figure 5a**). The authors also

noted that monosome-preferring transcripts had lower translation initiation and elongation rates. Here we used RCP-seq to directly assess initiation and elongation in neuronal-specific transcripts preferring monosomal or polysomal translation (Glock et al. 2021; Biever et al. 2020). Notably, for both soma and neuropil compartments, monosome-preferring transcripts showed lower SSU, 80S, and RNA abundance as compared to those that preferred polysomal translation (**Figures 5b and 5c**). Interestingly, while monosome-preferring transcripts showed lower TE than polysome-preferring transcripts from the neuropil compartment (**Figure 5d)**, they displayed similar levels of occupancy from scanning ribosomes (**Figure 5e**) coupled with a higher level of initiation (**Figure 5f**).

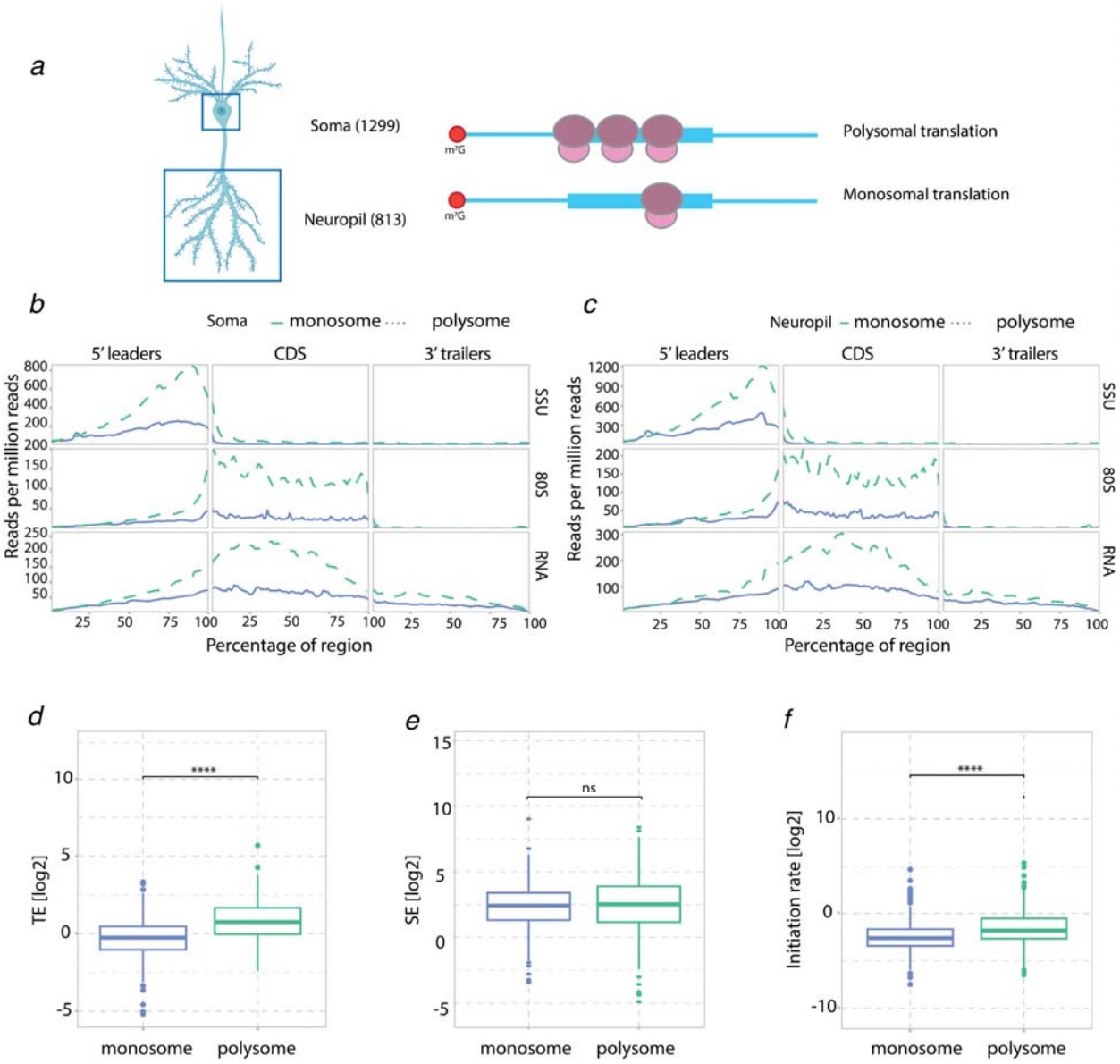

Figure 5: Translation landscape of neuropil and soma-enriched transcripts

a: Representation of neuronal compartments (soma and neuropil) with polysomal translation (multiple ribosomes elongating simultaneously) and of monosomal translation (only one ribosome elongating on the transcript). Numbers in parentheses indicate the number of genes used for analysis

b: Metagene coverage for transcripts enriched in the soma and preferring monosomal or polysomal translation.

c: Metagene coverage for transcripts enriched in the neuropil and preferring monosomal or polysomal translation.

d: Log_2 TE (FPKM, t-test statistics) for neuropil-enriched transcripts between the transcripts preferring monosomal or polysomal translation in the DG.

e: Log_2 SE (FPKM, t-test statistics) for neuropil-enriched transcripts between the transcripts preferring monosomal or polysomal translation in the DG.

f: Log_2 Initiation rate (FPKM, t-test statistics) for neuropil-enriched transcripts between the transcripts preferring monosomal or polysomal translation in the DG.

Mapping of SSU and 80S ribosomes in cortical tissue of adult mouse brain

To examine if RCP-seq with UV-crosslinking works for other brain tissues, we prepared SSU and 80S libraries from the cerebral cortex of the adult mouse brain (**Supplementary figures 3a and 3b**). The library quality was comparable to the DG (**Supplementary figure 3c-3i**). 37% of the SSU reads and 94% of the 80S reads mapped to the 5' leaders and CDS respectively (**Supplementary figure 3d**) and showed a strong enrichment relative to the expected distribution based on RNA (**Supplementary figure 3e**). Footprint length distributions were within the expected range with 20-75 nt for SSU and 28-32 nt for 80S (**Supplementary figure 3f**). Metagene heatmap of SSU footprints showed a diagonal of fragments (20-75 nt) preceding the TIS (**Supplementary figure 3g**) which is attributed to the longer pre-initiation complex conformations due to the presence of initiation factors (Bohlen et al. 2020; Archer et al. 2016). Surprisingly, we also observed a second, higher diagonal indicating a longer SSU conformation at the TIS (**Supplementary figures 3g**). This suggests that additional factors could be involved in the initiation of this configuration. For the 80S ribosomes **(Supplementary figures 3h and 3i)**, the footprints are enriched at the TIS and TTS and show the expected 3-nucleotide periodicity throughout the CDS. Together with the DG libraries, we were thus successful in applying RCP-seq to two different brain regions.

Discussion

Optimising RCP-seq for brain tissue

This study presents the first map of translation initiation dynamics in tandem with elongation in the mammalian brain. This was accomplished by adapting and optimising several steps in our previously published RCP-seq protocol for developing zebrafish embryos (Giess et al. 2020). While previous studies mapping SSUs to the mRNAs have used paraformaldehyde and chemicals such as dithiobis (succinimidyl propionate, DSP) (Wagner et al. 2022; Giess et al. 2020), the use of low (0.05%) PFA concentrations in the brain tissues gave poor yield of polysomes, possibly due to insufficient lysis of the tissue. To increase the amount of SSUs and to avoid the use of glycine to neutralise formaldehyde, we crosslinked ribosomal complex proteins to RNA using UV irradiation, used previously to map RBP binding sites and for

polysome profiling (Hafner et al. 2021; Darnell et al. 2011). A possible drawback of UV crosslinking of lysates could be the loss of SSUs during the lysis step. However, in our data we do not observe any such a loss and see a distribution of SSUs over the leaders similar to previous studies (Archer et al. 2016; Giess et al. 2020; Wagner et al. 2022). UV irradiation is also known to cause ribosome stress response (M. S. Iordanov et al. 1998; Mihail S. Iordanov et al. 2002), but this study exposes the lysates to UV and thereby bypasses the harmful effects of UV irradiation on tissue. Together these steps enabled us to successfully capture the transcriptome-wide occupancy of both scanning and elongating ribosome complexes from the DG and the cerebral cortex region of the mouse brain.

Our libraries of ribosomal occupancy from brain tissues were consistent with previously published datasets in terms of transcriptomic mapping, footprint length distributions, and 80S periodicity (Archer et al. 2016; Bohlen et al. 2020; Giess et al. 2020). Accordingly, we observed the diagonal preceding the TIS in the SSU libraries, which has been observed in all published RCP-seq and TCP-seq studies (Wagner et al. 2022; Giess et al. 2020). Interestingly, we observed a second diagonal in the cerebral cortex, indicating an approximately 10nt longer conformation present at the TIS. While sequencing data alone is insufficient to determine the factors present in this conformation, the read positions and lengths are indicative of the presence of one or more additional initiation factors downstream of the pre-initiation complex such as helicase eIF4A and its cofactor eIF4B as shown by recent structural evidence (Brito Querido et al. 2024).

Role of uORFs and SSU-poising in neuronal translation

A major finding of this study is the discovery of a distinct poised configuration of SSU enriched at the TIS. Previous studies from yeast and developing zebrafish embryos showed similar SSU patterns, but not in human cell line SSU libraries (Archer et al. 2016; Giess et al. 2020; Bohlen et al. 2020). This suggests that poising is a species or context-specific phenomenon. We introduced a metric to quantify this configuration relative to the initiating SSUs and showed that SSU poising is highly enriched in mRNAs found in the synaptic compartment, suggesting regulation of the transition from poised to initiating SSUs

in a subset of transcripts. In the mouse brain, SSU poising could be necessary for transcripts with slow elongation or start codon recognition rates or allow for fast and abundant translation in response to stimuli, such as during neuronal activity-induced bursts of protein synthesis. Supporting the later hypothesis, we find that genes with high SSU poising ratio show higher translation efficiency as compared to those with lower SSU posing. One of the interesting gene candidates is *CamkIIα*, which could undergo rapid translation upon synaptic stimulation (Håvik et al. 2003; Miller et al. 2002; Ostroff et al. 2002; Chirillo et al. 2019).

As discussed earlier (Archer et al. 2016), factors influencing and causing pile-up of SSUs may vary (e.g. mRNA sequence and structure, presence of IRES, SSU pausing) among transcripts. We observed that the presence of uORFs leads to less SSU poising, potentially by disassociating the SSUs after translation of the uORF. Similarly, the presence of uORFs can have an inhibitory effect on the translation of the downstream CDS. In line with previous reports (Calvo, Pagliarini, and Mootha 2009; Chew, Pauli, and Schier 2016; Johnstone, Bazzini, and Giraldez 2016), we observed globally a significant decrease in translational efficiency for transcripts harbouring a translated uORF (**Figure 3b)**.

Cell-type and compartment specific translation regulation

When subsetting on a previously published list of neuronal and glial enriched transcripts (Glock et al. 2021), we observed that neuronal genes are substantially more abundant, scanned and translated than glial transcripts. Furthermore, neuronal genes showed higher translation and scanning efficiencies than those belonging to the glial category. Focusing on transcripts that are predominantly monosomal or polysomal provided further mechanistic details on their translation regulation. Neuronal transcripts preferring polysome translation showed higher SSU and 80S occupancy, whereas monosome-preferring transcripts showed lower SSU and 80S reads, implying reduced recruitment of PIC to these transcripts in order to maintain a low initiation and elongation rate. Indeed, monosome-preferring transcripts showed lower initiation rates along with lower translation efficiencies, as compared to polysome-preferring transcripts. The evidence suggests that monosome-preferring transcripts are more sparsely or selectively

translated. The findings underscore the importance of transcriptome-wide mapping of both initiating and elongating ribosomes in providing an understanding of the plausible translation control mechanism of a specific pool of mRNAs.

Conclusion

While previous small ribosomal subunit studies have made use of samples from sources where abundant material has been available, such as yeast culture or cell lines, we here successfully adapted RCP-seq for small brain tissue samples (the mouse dentate gyrus). In tandem with total RNA and 80S analysis, we uncover cell type, and transcript-specific regulation at the scanning and elongation stages. We discover thousands of active uORFs and demonstrate their repressive function in the translation of the CDS. Additionally, we highlight a pattern of SSU poising upstream of the translation start site of synaptically enriched RNAs, identifying it as a possible regulatory step in translation underlying synapse maintenance and plasticity. We anticipate that future studies on scanning subunit occupancy will help to resolve long-standing questions on the role of initiation factors in the scanning process and how these influence the regulation of individual genes in mammalian brain function and dysfunction.

Materials and Methods

Animals

12 to 14-week-old C57BL/6 wild-type mice were used. Mice were bred and housed in their home cages. Room temperature (22◦C (±1◦C)) and relative humidity (46±5%) were maintained. Mice had free access to water and food and were maintained on a 12-hour light/dark cycle. This research is approved by the Norwegian National Research Ethics Committee in compliance with EU Directive 2010/63/EU, ARRIVE guidelines.

UV fixation of brain tissue and polysome profiling

Animals were anesthetized with urethane (1.5g/kg) and then sacrificed immediately. The whole brain was removed and positioned on a filter paper placed on a glass plate cooled with ice. After isolating both hippocampi, blood vessels and connective tissue were removed. The Cornu Ammonis (CA) region was separated from the dentate gyrus (DG) before placing the DG in microtubes in dry ice. After isolating both cerebral cortices, the white matter was carefully removed before placing the entire cortices in microtubes in dry ice. The brain samples were given a liquid nitrogen bath and then placed at -80 degrees Celsius for storage. It took a maximum of 10 minutes from sacrifice to sample storage to preserve RNA integrity. Long-term storage of tissue at -80 degrees Celsius was avoided to prevent RNA degradation.

Brain tissue was washed twice with ice-cold 1X PBS containing cycloheximide (0.1 mg/mL) before proceeding with the fixation/homogenisation. For formaldehyde fixation, whole tissues were incubated with 1ml formaldehyde solution for 5 min in ice. To neutralise formaldehyde, 1 M glycine was added and incubated for another 5 min. The tissue was then washed with 1X PBS twice before homogenisation. For UV crosslinking, the tissue was first lysed and the lysate was exposed to UV. Tissue homogenisation was done in lysis buffer (50mM Tris-Cl, pH 7.4; 100mM KCl; 5mM $MgCl_2$; EDTA-free protease inhibitor cocktail; 1mM DTT; 0.1mg/mL cycloheximide, 40U/ml Superase Inhibitor) in a dounce homogenizer with 15 strokes of loose pistol and 15 strokes of the tight piston on ice. The volume

of the lysis buffer used depended on the size of the tissue. For the cortex (one hemisphere), 0.5 mL was used. For DG regions, 0.3 mL was used. For one replicate, one cortical hemisphere (~17ug RNA) was used and 10 DGs (~9ug RNA) were used. The homogenate was transferred to an RNase-free 1.5 mL tube and 1% NP40 was added to the homogenate, mixed well, and incubated in ice for 10 min. The homogenate was spun at 2000 g for 10 min at 4 degrees Celsius. The clear supernatant (S1) was collected and then spun at 20000 g for 10 min at 4 degrees Celsius. The clear supernatant (S2) obtained was transferred to a 3.5 cm tissue culture dish placed on a bed of ice slush. The supernatant was UV cross-linked at 254 nm with 400 mJ/cm^2 three times in a CL-1000 ultraviolet crosslinker (UVP). The plate was swirled between each round of irradiation for uniform crosslinking. The RNA concentration was estimated by the absorbance using both qubit and nanodrop. This can be done before or after UV irradiation. The lysate was layered over a 10-50% sucrose gradient and spun at 40000 rpm for 2-4 hours at 4 degrees Celsius in an ultracentrifuge. The gradients were then run through a UV detector-fractionator (Biocomp).

Ribosome complex profiling sequencing

RNase digestion was done as previously described (Liu et al. 2019). 5U of RNase 1 was used for one unit of absorbance at A260 for a total volume of 300 μL lysate. RNase digestion for UV crosslinked lysates was done at 25 degrees Celsius for 45 min. The digestion was stopped by the addition of 50U of Superase Inhibitor. For total RNA sequencing, 50-100 μL of lysate was kept aside before the digestion step. 10-50% sucrose gradients (prepared in gradient buffer: 50mM Tris-Cl, pH7.4; 100mM KCl; 5mM $MgCl_2$; 1mM DTT) were made 45 min before the ultracentrifugation in polycarbonate tubes (Science Services, Germany, S7030). 450-500 μl of digested lysates were then layered over the gradients and run in SW41 Ti rotor at 40000 rpm for 3 hours. The gradients were then run through a UV detector-fractionator (Biocomp) and 20 fractions were collected. Fractions corresponding to the 40S and 80S peaks were used for RNA extraction and library preparation.

RNA extraction was done using TRIzol LS and in the final step, the RNA pellet was resuspended in 10 μl of nuclease-free water. The RNA sample was then run on a 15% polyacrylamide gel for size selection for the 40S and 80S footprints using RNA denaturing dye, with an ultra-low DNA ladder as the marker (Invitrogen: 10597012). For 40S footprints, gel from 20-80 nt was cut and for 80S footprints, gel from 20-50 nt was cut. The gel pieces were crushed and resuspended in 500 μl of 0.3M Sodium acetate solution overnight, at 4 degrees Celsius, and then filtered through 0.4 μm cellulose filters. RNA was pelleted overnight at -20 degrees Celsius in the presence of 2 μl of glycoblue and 375 μl isopropanol and resuspended in 10 μl of nuclease-free water. The size selected footprints were 3' dephosphorylated using PNK for 2 hours at 37 degrees Celsius in a final volume of 20 μl. After dephosphorylation, the RNA was concentrated and cleaned by the Oligo clean and concentrator kit (Zymo Research) in a final volume of 14 μl in nuclease-free water. The RNA footprints were then rRNA depleted with oligos from siTOOLS (riboPOOL riboseq h/m/r) and eluted in a final volume of 10 μl. Small RNA libraries were made using the Takara SMARTer smRNA kit and the manufacturer's protocol was followed. PCR cycles were based on the starting concentration of RNA. Total RNA libraries were prepared using the Takara SMARTer total RNA HI mammalian kit and the manufacturer's protocol was followed. Libraries containing primers or primer dimers were cleaned up using RNA XP clean-up beads (catalogue #A63987). The size and molarity of the libraries were estimated by obtaining bioanalyzer profiles (Agilent). Libraries were run as 100 bp single end on the NOVAseq 6000 platform up to a depth of 100M reads for each small RNA library or 30M reads for the total RNA library.

Ribosome complex profiling analysis

The repository at https://git.app.uib.no/valenlab/brain_dg_cortex_rcp contains all the code that was used for analysis and all of the processed data and figures are available there for inspection. All figures and processed tables are present in the repository. For the data processing, we used ORFik (1.19.3) as shown in the script "0_preprocess.R". Analysis uses the latest at the time, gencode mouse release M31 (GRCm39 v107). ORFik pipeline uses fastp software for trimming and STAR for alignment. Paired-end

fastq reads are initially aligned to the contaminants - phix, rRNA, ncRNA, tRNA, and finally to the genome. Important options that were set are adapter.sequence = "AAAAAAAAAA", trim.front = 3, min.length = 20. Aligned data is processed using ORFik and custom scripts available in the data repository. We restricted genes with multiple transcripts to a single transcript by selecting the one with the longest coding sequence. For statistical testing, we used cutoffs of log2 fold change of 1 or -1 and 0.05 as the significance level. Upstream ORFs were detected using the ORFik function “findUORFs” which by default searches for HTG start codons (not GAG), but we used only ATG as start codons. Furthermore, we filtered out these uORFs that don’t have any values over SSU/80S/RNA. We restricted further to one uORF per transcript by selecting the one with the highest translational efficiency.

For comparisons at the global-level, we calculate measures produced per library using FPKM values instead of raw counts and average replicates, furthermore, we normalise using reads per million reads for that particular group of genes to gain a comprehensive perspective. As we can see below, uORF measures are adapted from gene measures by changing the perspective of CDS to that of the uORF, and 5’ leader and 3’ trailer are becoming regions upstream/downstream of uORF CDS, but within boundaries of the transcript mRNA.

Formulae used in this study

Scanning efficiency (SE) = SSU on leaders / RNA on mRNA (leader + CDS + trailer)

Translation efficiency (TE) = 80S on CDS / RNA on mRNA

Initiation rate (IR) = 80S on CDS / SSU on leaders

uORF TE = 80S on uORF/ RNA on uORFs

uORF SSU consumption rate = SSU upstream of uORF / SSU downstream of uORF

uORF ratio = 80S of uORF / 80S of CDS

SSU poising: Short SSU (25-35nt) at -14: -12 relative to TIS / Long SSU (60-65nt) at -46: -36 relative to TIS

Poised SSUs/RNA: Long SSU (60-65nt) at -46: -36 relative to TIS/RNA on mRNA

Statistics

For boxplot figures t-test statistics were used to compare means of the distributions with corrected p-values using Benjamini-Hochberg methods.

Data availability

Raw reads are published under accession number PRJEB72224 in the European Nucleotide Archive.

Author contributions

PMK, FPP, EV and CRB designed the experiments. FPP performed the mice brain tissue dissection and PMK performed the ribosome complex profiling experiments. KL and EV conducted the bioinformatic analysis. PMK, KL and EV interpreted the data. All authors discussed the results and contributed to writing the manuscript.

Acknowledgements

FPP was funded by the L.Meltzers Høyskolefond 2022 - Ekstratildeling - for the project “Molecular control of protein synthesis underlying the plasticity of neural communication in the mammalian brain” (Project #103517122). Research in the CRB lab is supported by the Trond Mohn Research Foundation (TMS2021TMT04). PK and EV are funded by the Norwegian Cancer Society (Project #190290). The Genomics Core Facility (GCF) at the University of Bergen, which is a part of the NorSeq consortium, provided services on sequencing of small and total RNA libraries on NOVAseq 6000 platform; GCF is supported in part by major grants from the Research Council of Norway (grant no. 245979/F50) and Bergen Research Foundation (BFS) (grant no. BFS2017TMT04 and BFS2017TMT08)”.

References

Amorim, Inês S., Sonal Kedia, Stella Kouloulia, Konstanze Simbriger, Ilse Gantois, Seyed Mehdi Jafarnejad, Yupeng Li, et al. 2018. "Loss of eIF4E Phosphorylation Engenders Depression-like Behaviors via Selective mRNA Translation." *The Journal of Neuroscience: The Official Journal of the Society for Neuroscience* 38 (8): 2118–33.

Archer, Stuart K., Nikolay E. Shirokikh, Traude H. Beilharz, and Thomas Preiss. 2016. "Dynamics of Ribosome Scanning and Recycling Revealed by Translation Complex Profiling." *Nature* 535 (7613): 570–74.

Biever, Anne, Caspar Glock, Georgi Tushev, Elena Ciirdaeva, Tamas Dalmay, Julian D. Langer, and Erin M. Schuman. 2020. "Monosomes Actively Translate Synaptic mRNAs in Neuronal Processes." *Science* 367 (6477). https://doi.org/10.1126/science.aay4991.

Bohlen, Jonathan, Kai Fenzl, Günter Kramer, Bernd Bukau, and Aurelio A. Teleman. 2020. "Selective 40S Footprinting Reveals Cap-Tethered Ribosome Scanning in Human Cells." *Molecular Cell* 79 (4): 561–74.e5.

Bramham, Clive R., and David G. Wells. 2007. "Dendritic mRNA: Transport, Translation and Function." *Nature Reviews. Neuroscience* 8 (10): 776–89.

Brito Querido, Jailson, Masaaki Sokabe, Irene Díaz-López, Yuliya Gordiyenko, Christopher S. Fraser, and V. Ramakrishnan. 2024. "The Structure of a Human Translation Initiation Complex Reveals Two Independent Roles for the Helicase eIF4A." *Nature Structural & Molecular Biology* 31 (3): 455–64.

Calvo, Sarah E., David J. Pagliarini, and Vamsi K. Mootha. 2009. "Upstream Open Reading Frames Cause Widespread Reduction of Protein Expression and Are Polymorphic among Humans." *Proceedings of the National Academy of Sciences of the United States of America* 106 (18): 7507–12.

Cao, Ruifeng, Christos G. Gkogkas, Nuria de Zavalia, Ian D. Blum, Akiko Yanagiya, Yoshinori Tsukumo, Haiyan Xu, et al. 2015. "Light-Regulated Translational Control of Circadian Behavior by eIF4E Phosphorylation." *Nature Neuroscience* 18 (6): 855–62.

Chew, Guo-Liang, Andrea Pauli, and Alexander F. Schier. 2016. "Conservation of uORF Repressiveness and Sequence Features in Mouse, Human and Zebrafish." *Nature Communications* 7 (May):11663.

Chirillo, Michael A., Mikayla S. Waters, Laurence F. Lindsey, Jennifer N. Bourne, and Kristen M. Harris. 2019. "Local Resources of Polyribosomes and SER Promote Synapse Enlargement and Spine Clustering after Long-Term Potentiation in Adult Rat Hippocampus." *Scientific Reports* 9 (1): 3861.

Darnell, Jennifer C., Sarah J. Van Driesche, Chaolin Zhang, Ka Ying Sharon Hung, Aldo Mele, Claire E. Fraser, Elizabeth F. Stone, et al. 2011. "FMRP Stalls Ribosomal Translocation on mRNAs Linked to Synaptic Function and Autism." *Cell* 146 (2): 247–61.

Dever, Thomas E., Ivaylo P. Ivanov, and Alan G. Hinnebusch. 2023. "Translational Regulation by uORFs and Start Codon Selection Stringency." *Genes & Development* 37 (11-12): 474–89.

Giess, Adam, Yamila N. Torres Cleuren, Håkon Tjeldnes, Maximilian Krause, Teshome Tilahun Bizuayehu, Senna Hiensch, Aniekan Okon, Carston R. Wagner, and Eivind Valen. 2020. "Profiling of Small Ribosomal Subunits Reveals Modes and Regulation of Translation Initiation." *Cell Reports* 31 (3): 107534.

Glock, Caspar, Anne Biever, Georgi Tushev, Belquis Nassim-Assir, Allison Kao, Ina Bartnik, Susanne Tom Dieck, and Erin M. Schuman. 2021. "The Translatome of Neuronal Cell Bodies, Dendrites, and Axons." *Proceedings of the National Academy of Sciences of the United States of America* 118 (43). https://doi.org/10.1073/pnas.2113929118.

Hafner, Markus, Maria Katsantoni, Tino Köster, James Marks, Joyita Mukherjee, Dorothee Staiger, Jernej Ule, and Mihaela Zavolan. 2021. "CLIP and Complementary Methods." *Nature Reviews Methods Primers* 1 (1): 1–23.

Håvik, Bjarte, Håvard Røkke, Kjetil Bårdsen, Svend Davanger, and Clive R. Bramham. 2003. "Bursts of

High-Frequency Stimulation Trigger Rapid Delivery of Pre-Existing Alpha-CaMKII mRNA to Synapses: A Mechanism in Dendritic Protein Synthesis during Long-Term Potentiation in Adult Awake Rats." *The European Journal of Neuroscience* 17 (12): 2679–89.

Hien, Annie, Gemma Molinaro, Botao Liu, Kimberly M. Huber, and Joel D. Richter. 2020. "Ribosome Profiling in Mouse Hippocampus: Plasticity-Induced Regulation and Bidirectional Control by TSC2 and FMRP." *Molecular Autism* 11 (1): 78.

Hinnebusch, Alan G. 2014. "The Scanning Mechanism of Eukaryotic Translation Initiation." *Annual Review of Biochemistry* 83 (January):779–812.

Holt, Christine E., Kelsey C. Martin, and Erin M. Schuman. 2019. "Local Translation in Neurons: Visualization and Function." *Nature Structural & Molecular Biology* 26 (7): 557–66.

Ingolia, Nicholas T., Sina Ghaemmaghami, John R. S. Newman, and Jonathan S. Weissman. 2009. "Genome-Wide Analysis in Vivo of Translation with Nucleotide Resolution Using Ribosome Profiling." *Science* 324 (5924): 218–23.

Iordanov, Mihail S., Remy J. Choi, Olga P. Ryabinina, Thanh-Hoai Dinh, Robert K. Bright, and Bruce E. Magun. 2002. "The UV (Ribotoxic) Stress Response of Human Keratinocytes Involves the Unexpected Uncoupling of the Ras-Extracellular Signal-Regulated Kinase Signaling Cascade from the Activated Epidermal Growth Factor Receptor." *Molecular and Cellular Biology* 22 (15): 5380–94.

Iordanov, M. S., D. Pribnow, J. L. Magun, T. H. Dinh, J. A. Pearson, and B. E. Magun. 1998. "Ultraviolet Radiation Triggers the Ribotoxic Stress Response in Mammalian Cells." *The Journal of Biological Chemistry* 273 (25): 15794–803.

Johnstone, Timothy G., Ariel A. Bazzini, and Antonio J. Giraldez. 2016. "Upstream ORFs Are Prevalent Translational Repressors in Vertebrates." *The EMBO Journal* 35 (7): 706–23.

Kute, Preeti Madhav, Omar Soukarieh, Håkon Tjeldnes, David-Alexandre Trégouët, and Eivind Valen. 2021. "Small Open Reading Frames, How to Find Them and Determine Their Function." *Frontiers in Genetics* 12:796060.

Larsson, Ola, Bin Tian, and Nahum Sonenberg. 2013. "Toward a Genome-Wide Landscape of Translational Control." *Cold Spring Harbor Perspectives in Biology* 5 (1): a012302.

Liu, Botao, Gemma Molinaro, Huan Shu, Emily E. Stackpole, Kimberly M. Huber, and Joel D. Richter. 2019. "Optimization of Ribosome Profiling Using Low-Input Brain Tissue from Fragile X Syndrome Model Mice." *Nucleic Acids Research* 47 (5): e25.

Merrick, William C., and Graham D. Pavitt. 2018. "Protein Synthesis Initiation in Eukaryotic Cells." *Cold Spring Harbor Perspectives in Biology* 10 (12). https://doi.org/10.1101/cshperspect.a033092.

Miller, Stephan, Masahiro Yasuda, Jennifer K. Coats, Ying Jones, Maryann E. Martone, and Mark Mayford. 2002. "Disruption of Dendritic Translation of CaMKIIα Impairs Stabilization of Synaptic Plasticity and Memory Consolidation." *Neuron* 36 (3): 507–19.

Moon, Stephanie L., Nahum Sonenberg, and Roy Parker. 2018. "Neuronal Regulation of eIF2α Function in Health and Neurological Disorders." *Trends in Molecular Medicine* 24 (6): 575–89.

Oliveira, Mauricio M., and Eric Klann. 2022. "eIF2-Dependent Translation Initiation: Memory Consolidation and Disruption in Alzheimer's Disease." *Seminars in Cell & Developmental Biology* 125 (May):101–9.

Ostroff, Linnaea E., John C. Fiala, Brenda Allwardt, and Kristen M. Harris. 2002. "Polyribosomes Redistribute from Dendritic Shafts into Spines with Enlarged Synapses during LTP in Developing Rat Hippocampal Slices." *Neuron* 35 (3): 535–45.

Patil, Sudarshan, Kleanthi Chalkiadaki, Tadiwos F. Mergiya, Konstanze Krimbacher, Inês S. Amorim, Shreeram Akerkar, Christos G. Gkogkas, and Clive R. Bramham. 2023. "eIF4E Phosphorylation Recruits β-Catenin to mRNA Cap and Promotes Wnt Pathway Translation in Dentate Gyrus LTP Maintenance." *iScience*. https://www.cell.com/iscience/pdf/S2589-0042(23)00726-5.pdf.

Sharma, Vijendra, Rapita Sood, Abdessattar Khlaifia, Mohammad Javad Eslamizade, Tzu-Yu Hung, Danning Lou, Azam Asgarihafshejani, et al. 2020. "eIF2α Controls Memory Consolidation via Excitatory and Somatostatin Neurons." *Nature* 586 (7829): 412–16.

Sokabe, Masaaki, and Christopher S. Fraser. 2019. “Toward a Kinetic Understanding of Eukaryotic Translation.” *Cold Spring Harbor Perspectives in Biology* 11 (2). https://doi.org/10.1101/cshperspect.a032706.

Sun, Chao, and Erin Schuman. 2023. “A Multi-Omics View of Neuronal Subcellular Protein Synthesis.” *Current Opinion in Neurobiology* 80 (June):102705.

Thomson, Sophie R., Sang S. Seo, Stephanie A. Barnes, Susana R. Louros, Melania Muscas, Owen Dando, Caoimhe Kirby, et al. 2017. “Cell-Type-Specific Translation Profiling Reveals a Novel Strategy for Treating Fragile X Syndrome.” *Neuron* 95 (3): 550–63.e5.

Wagner, Susan, Jonathan Bohlen, Anna Herrmannova, Jan Jelínek, Thomas Preiss, Leoš Shivaya Valášek, and Aurelio A. Teleman. 2022. “Selective Footprinting of 40S and 80S Ribosome Subpopulations (Sel-TCP-Seq) to Study Translation and Its Control.” *Nature Protocols* 17 (10): 2139–87.

Wagner, Susan, Anna Herrmannová, Vladislava Hronová, Stanislava Gunišová, Neelam D. Sen, Ross D. Hannan, Alan G. Hinnebusch, Nikolay E. Shirokikh, Thomas Preiss, and Leoš Shivaya Valášek. 2020. “Selective Translation Complex Profiling Reveals Staged Initiation and Co-Translational Assembly of Initiation Factor Complexes.” *Molecular Cell* 79 (4): 546–60.e7.